Photonic Generation of a Windowed Phase-Coded Microwave Waveform With Suppressed Spectrum Sidelobes

Yang Hu, Erwin H. W. Chan, *Senior Member, IEEE*, Xudong Wang, Xinhuan Feng, Bai-Ou Guan, *Fellow, Optica*, and Jianping Yao, *Fellow, IEEE, Fellow, Optica*

***Abstract*—An approach to photonic generation of a windowed binary phase-coded microwave waveform with suppressed spectrum sidelobes is proposed and demonstrated. An optical double sideband plus carrier signal with the carrier and the two sidebands being orthogonally polarized is generated by a dual-polarization quadrature phase shift keying (DP-QPSK) modulator, with the generated signal sent to a phase modulator (PM) where phase coding is performed. The PM can support phase modulation in two orthogonal polarization directions. The phase-modulated signals are projected to one polarization direction and detected at a photodetector (PD). Switching the polarity of the coding signal, a π phase shift is introduced. Since the amplitude of the generated signal is dependent on the amplitude of the input coding signal, a windowing function is applied to the generated waveform by using a windowed input phase coding signal, to suppress the sidelobes in the spectrum of the generated microwave waveform. The key features of the proposed waveform generator include all-optical generation without the need of electronic components and optical filters, thus ensuring a wide operating frequency range. The proposed phase-coded microwave waveform generator also has the ability to switch between the fundamental and harmonic carrier frequency by controlling the modulator bias voltages. Experimental results show that, using a windowed 64-bit Gaussian pseudo-random binary sequence coding signal, a phase-coded microwave waveform is generated with the sidelobes of the spectrum largely suppressed by 20 dB and a pulse compression ratio as large as 133. Generation of binary phase-coded microwave waveforms at the 2nd harmonic carrier frequencies is also demonstrated experimentally.**

Manuscript received 20 January 2022; revised 26 March 2022; accepted 13 April 2022. Date of publication 19 April 2022; date of current version 21 October 2022. This work was supported in part by Guangdong Province Key Field R&D Program Project under Grant 2020B0101110002, in part by the National Natural Science Foundation of China under Grants 61860206002 and 61771221, and in part by the National Key R&D Program of China under Grant 2021YFB2800804. *(Corresponding authors: Xudong Wang; Xinhuan Feng.)*

Yang Hu, Xudong Wang, Xinhuan Feng, and Bai-Ou Guan are with the Guangdong Provincial Key Laboratory of Optical Fiber Sensing and Communications, Institute of Photonics Technology, Jinan University, Guangzhou 510632, China (e-mail: hyhy19971210@stu2019.jnu.edu.cn; txudong.wang@email.jnu.edu.cn; eexhfeng@gmail.com; guanboo@yahoo.com).

Erwin H. W. Chan is with the College of Engineering, IT and Environment, Charles Darwin University, Darwin, NT 0909, Australia (e-mail: erwin.chan@cdu.edu.au).

Jianping Yao is with the Guangdong Provincial Key Laboratory of Optical Fiber Sensing and Communications, Institute of Photonics Technology, Jinan University, Guangzhou 510632, China, and also with the Microwave Photonics Research Laboratory, School of Electrical Engineering and Computer Science, University of Ottawa, Ottawa, ON K1N 6N5, Canada (e-mail: jpyao@uottawa.ca).

Color versions of one or more figures in this article are available at https://doi.org/10.1109/JLT.2022.3168065.

Digital Object Identifier 10.1109/JLT.2022.3168065

***Index Terms*—Frequency multiplication, microwave photonics, phase coding, photonic signal generation, pulse compression.**

I. Introduction

PHASE-CODED microwave waveforms are widely used in radio ranging and imaging systems in which pulse compression can be implemented to improve the range or imaging resolution [1]. A phase-coded microwave signal can be generated electronically. A conventional electronic approach to generate a phase-coded microwave waveform is to inject a microwave carrier into an electrical phase modulator driven by a coding signal. Such an approach is simple and with low loss. However, electrical phase modulators, compared with optical modulators, have smaller bandwidth. For example, the bi-phase modulator from Fairview Microwave can operate at 26.5–40 GHz and the phase modulator from Planar Monolithics Industries can operate at 18–40 GHz while an electro-optic modulator can operate from DC to over 100 GHz [2]. More importantly, the electrical phase modulators have a slow switching speed of more than 50 ns. Hence, they cannot be used to generate phase-coded microwave waveforms in which the coding signal has a bandwidth of hundreds of MHz or GHz. Thus, it is advantageous to generate phase-coded microwave waveforms based on photonic techniques. Other than the requirements for a high operating frequency and wide bandwidth, high reconfigurability is also a feature widely needed by microwave waveform generation systems, which can be achieved based on photonic techniques. In addition, microwave waveform generators implemented based on photonic techniques have other features including immunity to electromagnetic interference and parallel processing capabilities [3], [4].

Recently, a number of photonic-assisted phase-coded microwave waveform generators have been reported. A phase-coded microwave waveform can be produced based on direct space-to-time pulse shaping [5], photonic microwave delay-line filtering [6], and spectral shaping and frequency-to-time (SS-FTT) mapping [7]. The limitation of these approaches is that the carrier frequency of the generated phase-coded signals cannot be tuned or is hard to tune. To generate a phase-coded microwave waveform with a tunable carrier frequency, one may impose phase coding to one optical wavelength, by beating the phase-coded wavelength with another unmodulated optical

wavelength, a frequency-tunable phase-coded microwave signal can be generated [8]–[11]. By switching between the opposite quadrature biasing points of a Mach-Zehnder modulator (MZM), a frequency tunable binary phase-coded microwave waveform can also be generated [12]. For these phase-coded microwave waveform generators reported in [5]–[12], the phase information encoded on the generated microwave waveform is proportional to the amplitude of the phase coding signal, thus it is not possible to apply a windowing function to the waveform, to tailor the spectrum to reduce spectrum sidelobes. For many applications, however, it is highly desired that a phase-coded microwave waveform has a band-limited spectrum with ultra-low spectrum sidelobes, to reduce possible interferences with other wireless systems, such as satellite, cellular communications, and GPS systems [13]. A solution of generating a phase-coded microwave signal with suppressed spectrum sidelobes is to apply a windowing function to the microwave waveform without affecting the encoded phase information.

Recently, we have proposed a technique to generate a phase-coded microwave waveform with suppressed spectrum sidelobes, which was presented at MWP2021 [14]. This paper is an extension of the work reported [14], in which more details about the system analysis and experiments are provided. For the last few years, numerous approaches have been proposed for the generation of phase-coded microwave waveforms [5]–[12]. In general, the phase information in a phase-coded microwave waveform is encoded by using a phase coding signal and the phase information is proportional to the amplitude of the phase coding signal. Since the amplitude of a phase coding signal contains the phase information, it is not possible to use a windowing function to control the spectrum sidelobes. The key novelty of this approach, however, is that the phase information encoded on a microwave carrier is not dependent on the amplitude of the phase coding signal, thus it provides an additional degree of freedom which can be used to apply a windowing function to a phase-coded microwave waveform to reduce the spectrum sidelobes. In addition, a windowed microwave waveform has a broadened spectrum, the pulse compression ratio (PCR) is also increased. Some preliminary results have been reported in [14]. In this paper, more details including system analysis and experiments to show the generation of a fundamental and a second harmonic phase-coded microwave waveform is provided. The frequency tunability is also demonstrated.

II. Topology

Fig. 1(a) shows the structure of the proposed all-optical binary phase-coded microwave waveform generator [14]. A dual-polarization quadrature phase shift keying (DP-QPSK) modulator and a phase modulator (PM) are employed in the system. The DP-QPSK modulator consists of two QPSK modulators connected in parallel and a 90° polarization rotator at the output of the bottom QPSK modulator, as shown in Fig. 1(b). Each QPSK modulator has a main MZM and two sub-MZMs with each sub-MZM having an RF port. An RF tone with an angular frequency ω_{RF} is applied to a sub-MZM (MZM1) of

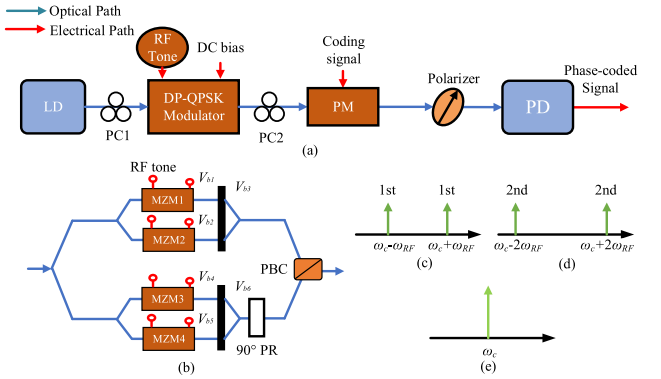

Fig. 1. (a) Schematic diagram of the proposed system for generating a binary phase-coded microwave waveform with suppressed spectrum sidelobes. (b) Structure of a DP-QPSK modulator. The upper QPSK modulator is biased to generate (c) two first order sidebands or (d) two second order sidebands. (e) Only the optical carrier is obtained at the output of the lower QPSK modulator. LD: laser diode; DP-QPSK: dual-polarization quadrature phase shift keying; MZM: Mach-Zehnder modulator; PBC: polarization beam combiner; PM: phase modulator; 90° PR: 90° polarization rotator.

the upper QPSK modulator. The operating point of each MZM is controlled by a DC bias voltage. By controlling the three bias voltages (V_{b1}, V_{b2} and V_{b3}) of the upper QPSK modulator to allow the two sub-MZMs and the main MZM all to operate at the null points, a pair of the first order sidebands at $\omega_c \pm \omega_{RF}$ with the carrier being fully suppressed are generated, as shown in Fig. 1(c). Alternatively, the three bias voltages (V_{b1}, V_{b2} and V_{b3}) can be set such that the two sub-MZMs and the main MZM operate at the peak, close to peak, and null point, respectively. In this case, instead of having a pair of the first order sidebands, a pair of the second order sidebands at $\omega_c \pm 2\omega_{RF}$ are present at the output of the upper QPSK modulator, as shown in Fig. 1(d). No RF tone or signal is applied to the lower QPSK modulator. The two MZMs (MZM3 and MZM4) in the lower QPSK modulator are biased at the peak and null points, respectively. Therefore, the continuous wave (CW) light from the laser diode (LD) only passes through MZM3. Its phase can be controlled by adjusting the bias voltage V_{b6} to the main MZM in the lower QPSK modulator.

At the DP-QPSK modulator output, an optical double-sideband plus carrier (DSB+C) signal with the carrier and the two sidebands being orthogonally polarized is generated. The generated optical signal is sent to the PM. Note that the PM used in the system here can support phase modulation in two orthogonal polarization directions with different phase modulation indices [15]. A phase coding signal is applied to the PM to generate orthogonally polarized phase-modulated signals. By projecting the two orthogonally polarized phase-modulated signals to one polarization direction using a polarizer and detecting at a photodetector (PD), a binary phase-coded microwave waveform with π phase shift is generated. Note that the π phase shift is introduced to the generated microwave waveform by switching the polarity of the phase coding signal, rather than the amplitude of the phase coding signal, thus, it is possible to apply a windowing function through changing the amplitude of

the phase coding signal to the generated microwave waveform, to reduce the spectrum sidelobes.

III. Principle of Operation and Analysis

Referring to Fig. 1(a), the sub-MZMs (MZM1-MZM4) in the DP-QPSK modulator are operating in the push-pull configuration [16]. When MZM1 is driven by an RF tone with an angular frequency ω_{RF}, and MZM3 and MZM4 are biased at the peak and null point, respectively, the electric fields at the outputs of the upper and lower QPSK modulators ($E_{up,QPSK}$ and $E_{low,QPSK}$) are given by (1) and (2) respectively. E_{in} is the electric field amplitude of the CW light into the DP-QPSK modulator, $J_n(x)$ is the Bessel function of the *n*th order of the first kind, $\beta_{RF} = \pi V_{RF}/V_{\pi,RF}$ is the modulation index, V_{RF} is the voltage of the RF tone into MZM1, $V_{\pi,RF}$ is the modulator RF port switching voltage, $\beta_{bn} = \pi V_{bn}/V_{\pi,DC}$ is the bias angle introduced by the bias voltage V_{bn}, $V_{\pi,DC}$ is the modulator DC port switching voltage, and θ is the phase difference caused by a slight length difference between the upper and lower path of the DP-QPSK modulator. Note that only the optical carrier and the first and second order sidebands are considered in (1). The higher order sidebands can be neglected under small signal modulation condition. The signal at the output of the lower QPSK modulator passes through the 90° polarization rotator and combines with the signal at the output of the upper QPSK modulator via the polarization beam combiner (PBC). $E_{up,QPSK}$ and $E_{low,QPSK}$ are orthogonal at the output of the DP-QPSK modulator. Hence, the electric field at the output of the DP-QPSK modulator can be written as

$$E_{out,DP-QPSK} = \begin{bmatrix} E_{up,QPSK} \cdot \overrightarrow{e_x} \\ E_{low,QPSK} \cdot \overrightarrow{e_y} \end{bmatrix} \tag{3}$$

where $\overrightarrow{e_x}$ and $\overrightarrow{e_y}$ represent the two orthogonal polarization states. The two orthogonally polarized optical signals are sent to the PM, which is driven by a phase coding signal to phase modulate the optical signals. The electric field at the output of the PM can be written as

$$E_{out,PM} = \begin{bmatrix} E_{up,QPSK} e^{j\beta_c s(t)} \cdot \overrightarrow{e_x} \\ E_{low,QPSK} e^{j\gamma\beta_c s(t)} \cdot \overrightarrow{e_y} \end{bmatrix} \tag{4}$$

where $\beta_c = \pi V_c/V_{\pi,PM}$ is the modulation index, V_c is the peak-to-peak amplitude of the phase coding signal, $V_{\pi,PM}$ is the PM switching voltage, $s(t)$ is the normalized phase coding signal with an unit amplitude, and γ is the modulation index ratio between the TE and TM modes, which is approximately 0.33 for a $LiNbO_3$ crystal [17]. A polarizer with its principal axis aligns at an angle of 45° to one of the principal axes of the PM is connected to the output of the PM. The electric field of the optical signal after the linear polarizer can be expressed as [18]

$$E_{out} = \frac{\sqrt{2}}{2}\left[E_{up,QPSK} e^{j\beta_c s(t)} + E_{low,QPSK} e^{j\gamma\beta_c s(t)}\right] \tag{5}$$

The bias voltages (V_{b1}, V_{b2}, V_{b3} and V_{b6}) are designed such that MZM1 and MZM2 are biased at the null point, i.e., $\beta_{b1} = \beta_{b2} = \pi/2$, the main MZM of the upper QPSK modulator is also biased at the null point, i.e., $\beta_{b3} = \pi$, and $\beta_{b6} = \pi/2\text{-}\theta$. Thus, (5) can be re-written as

$$E_{out} = \frac{1}{4} E_{in} e^{j\left(\omega_c t + \frac{\pi}{2}\right)} \times \left\{ \begin{matrix} \left[J_1(\beta_{RF})\, e^{j\omega_{RF}t} + J_{-1}(\beta_{RF})\, e^{-j\omega_{RF}t}\right] e^{j\beta_c s(t)} \\ + e^{j\gamma\beta_c s(t)} \end{matrix} \right\} \tag{6}$$

The output photocurrent can be obtained from (6) and is given by

$$\begin{aligned} I_{out} &= \Re E_{out} E_{out}^* \\ &= \frac{1}{16}\Re P_{in}\begin{bmatrix} 1 + 2J_1^2(\beta_{RF}) - 2J_1^2(\beta_{RF})\cos(2\omega_{RF}t) \\ + 4J_1(\beta_{RF})\sin[(\gamma-1)\beta_c s(t)]\sin(\omega_{RF}t) \end{bmatrix} \end{aligned} \tag{7}$$

where $\Re$ is the responsivity of the PD and P_{in} is the optical power of the CW light into the DP-QPSK modulator. The last term in (7) is a phase-coded signal at the frequency of the input RF tone. Similarly, when MZM1 and MZM2 are biased at the peak point and close to the peak point, i.e., $\beta_{b1} = 0$ and $\beta_{b2} = \cos^{-1}(J_0(\beta_{RF})) \approx 0$, the main MZM of the upper QPSK modulator is biased at the null point, i.e., $\beta_{b3} = \pi$, and $\beta_{b6} = \pi/2\text{-}\theta$, (5) can be re-written as

$$E_{out} = \frac{1}{4} E_{in} e^{j(\omega_c t)} \times \left\{ \begin{matrix} \left[J_2(\beta_{RF})\, e^{j2\omega_{RF}t} + J_{-2}(\beta_{RF})\, e^{-j2\omega_{RF}t}\right] e^{j\beta_c s(t)} \\ + e^{j\frac{\pi}{2}} e^{j\gamma\beta_c s(t)} \end{matrix} \right\} \tag{8}$$

In this case, the photocurrent becomes

$$\begin{aligned} I_{out} &= \Re E_{out} E_{out}^* \\ &= \frac{1}{16}\Re P_{in}\begin{bmatrix} 1 + 2J_2^2(\beta_{RF}) + 2J_2^2(\beta_{RF})\cos(4\omega_{RF}t) \\ - 4J_2(\beta_{RF})\sin[(\gamma-1)\beta_c s(t)]\cos(2\omega_{RF}t) \end{bmatrix} \end{aligned} \tag{9}$$

$$E_{up,QPSK} = \frac{\sqrt{2}}{4} E_{in} e^{j\omega_c t} \cdot \begin{bmatrix} \cos(\beta_{b1})\, J_0(\beta_{RF}) \\ + \sin(\beta_{b1})\, J_1(\beta_{RF})\, e^{j\left(\omega_{RF}t + \frac{\pi}{2}\right)} + \sin(\beta_{b1})\, J_{-1}(\beta_{RF})\, e^{-j\left(\omega_{RF}t - \frac{\pi}{2}\right)} \\ + \cos(\beta_{b1})\, J_2(\beta_{RF})\, e^{2j\omega_{RF}t} + \cos(\beta_{b1})\, J_{-2}(\beta_{RF})\, e^{-2j\omega_{RF}t} \\ + \cos(\beta_{b2}) \cdot e^{j\beta_{b3}} \end{bmatrix} \tag{1}$$

$$E_{low,QPSK} = \frac{\sqrt{2}}{4} E_{in} e^{j(\omega_c t + \theta)} e^{j\beta_{b6}} \tag{2}$$

TABLE I
BIAS ANGLES OF THE SUB-MZMS AND MAIN-MZMS INSIDE THE DP-QPSK MODULATOR REQUIRED TO OBTAIN A PHASE-CODED MICROWAVE PULSE SIGNAL AT THE FUNDAMENTAL OR TWICE THE FREQUENCY OF THE INPUT RF TONE

Bias angle	Fundamental-frequency phase-coded signal	Doubled-frequency phase-coded signal
β_{b1}	$\pi/2$	0
β_{b2}	$\pi/2$	$\cos^{-1}(J_0(\beta_{RF}))\approx 0$
β_{b3}	π	π
β_{b4}	0	0
β_{b5}	$\pi/2$	$\pi/2$
β_{b6}	$\pi/2$-θ	$\pi/2$-θ

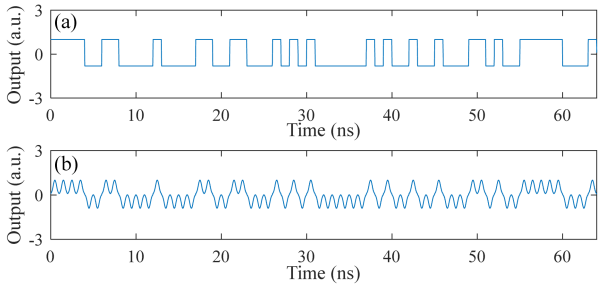

Fig. 2. 1 Gbit/s 64-bit PRBS coding signals (a) without and (b) with Gaussian windowing.

The last term in (9) is the phase-coded microwave signal at twice the frequency of the input RF tone. This shows that a phase-coded microwave signal at the fundamental or the 2nd harmonic RF frequency can be generated by simply controlling the DP-QPSK modulator bias voltages.

Table I summarizes the bias angles of the sub and main MZMs inside the DP-QPSK modulator required to generate a phase-coded microwave signal at the fundamental and the harmonic RF frequency. It can be seen from Table I that the fundamental and frequency-doubled phase-coded signal can be switched by controlling only two bias voltages of the DP-QPSK modulator. Note from (7) and (9) that the system also generates a DC component and an RF tone at the second or fourth harmonic frequency. When there is no phase coding signal into the system, i.e., $s(t) = 0$, only a DC component and a small-amplitude RF tone at the harmonic frequency are generated. When a phase coding signal is applied to the system and its polarity is changed (that is, the amplitude is changed from a positive/negative to negative/positive), there is a π phase shift in the generated phase-coded microwave waveform. This is the key to generate a binary phase-coded microwave signal with the coded phase being independent of the amplitude of the phase coding signal. Thanks to the unique property of this approach, the amplitude of the phase coding signal can be changed to apply a windowing function to the generated phase-coded microwave signal to tailor its spectrum. If a Gaussian window is applied, the sidelobes of the spectrum can be significantly suppressed.

A Gaussian function is given by [13]

$$W(t) = e^{-\frac{t^2}{2\delta^2}} \tag{10}$$

where δ is the standard deviation, which is inversely proportional to the width factor. Using a Gaussian-windowed coding signal with a width factor of 2.5, the first sidelobe in the output phase-coded signal spectrum is 44 dB below the mainlobe. This corresponds to 31-dB improvement in sidelobe suppression compared with that when using a conventional square wave coding signal. Due to the high sidelobe suppression, the phase-coded signal generated using a Gaussian-windowed coding signal is highly band-limited.

The operation of the phase-coded microwave waveform generator shown in Fig. 1(a) is first studied by simulations. The DP-QPSK modulator is driven by a 4 GHz RF tone. The PM, which supports both TE and TM modes, is emulated by using a polarization beam splitter (PBS), two PMs and a PBC, to split the orthogonally polarized sidebands and carrier from the DP-QPSK modulator, connecting the PBS outputs to the two PMs with different modulation efficiencies, and using the PBC to combine the two PM outputs. The two PMs are driven by a 1 Gbit/s 64-bit pseudo-random binary sequence (PRBS) code followed by 22 "0" bits. Fig. 2(a) and (b) shows two phase coding signals without and with Gaussian windowing, both with a 64-ns duration. The width factor of the Gaussian function is 2.5. A linear polarizer is connected after the PBC. The output signal is monitored using a signal analyzer module connected to the PD output.

Firstly, the bias voltages of the sub-MZMs and the main-MZMs in the DP-QPSK modulator are set to obtain the bias angles, as shown in Table I, for generating a phase-coded signal at the fundamental frequency of the input RF tone. The modulation index β_{RF} is set at 0.2. Fig. 3(a) and (b) shows the electrical spectra of the generated binary phase-coded microwave pulse signals when the input is a square wave coding signal and a Gaussian-windowed coding signal, respectively. As can be seen the sidelobes are largely suppressed to below the system noise floor when a Gaussian-windowing function is applied. Note that the width of the mainlobe is increased when a Gaussian windowing function is applied. It is known that an increase in the spectrum width would lead to a reduction in the pulse width in the time domain. Fig. 3(c) and (d) shows the autocorrelations of the phase-coded microwave signal without and with a Gaussian windowing function. The pulse widths are 1.02 ns and 0.48 ns, with the corresponding PCRs being 62 and 132, respectively, demonstrating an increase in the PCR by over 2 times thanks to the increase in the spectrum width when applying a Gaussian windowing function to the generated microwave waveform.

Next, the bias angles of the sub-MZMs and the main-MZMs in the DP-QPSK modulator are set, as shown in Table I, to obtain a frequency-doubled phase-coded microwave waveform. Fig. 4(a) and (b) shows the electrical spectra of the generated frequency-doubled phase-coded microwave pulse signals when the input is a square wave coding signal and a Gaussian-windowed coding signal, respectively. As can be seen the sidelobes are largely suppressed to below the system noise floor when a Gaussian-windowing function is applied. Again, the width of the mainlobe is increased when a Gaussian windowing function is applied. Fig. 4(c) and (d) shows the autocorrelations of the

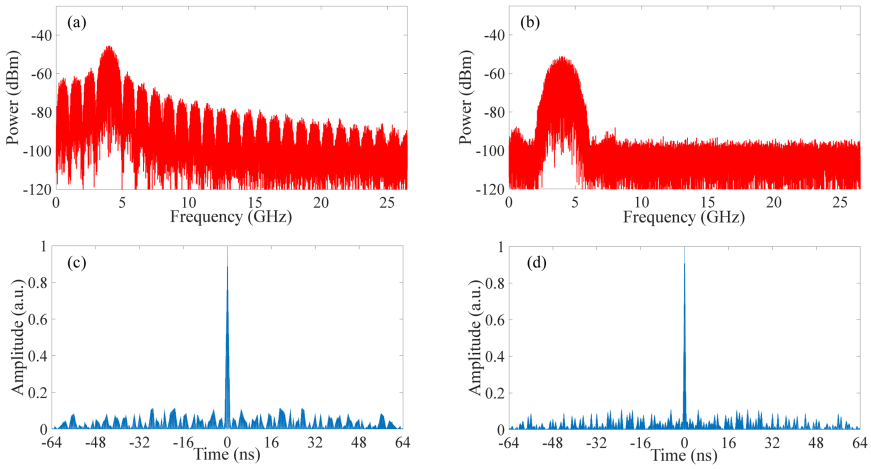

Fig. 3. Simulated electrical spectra of the binary phase-coded microwave signal at the fundamental frequency and the autocorrelation. (a) Spectrum when a square wave windowing function is applied. (b) Spectrum when a Gaussian windowing function is applied. (c) Autocorrelation of the generated microwave waveform when a square wave windowing function is applied. (d) Autocorrelation of the generated microwave waveform when a Gaussian windowing function is applied.

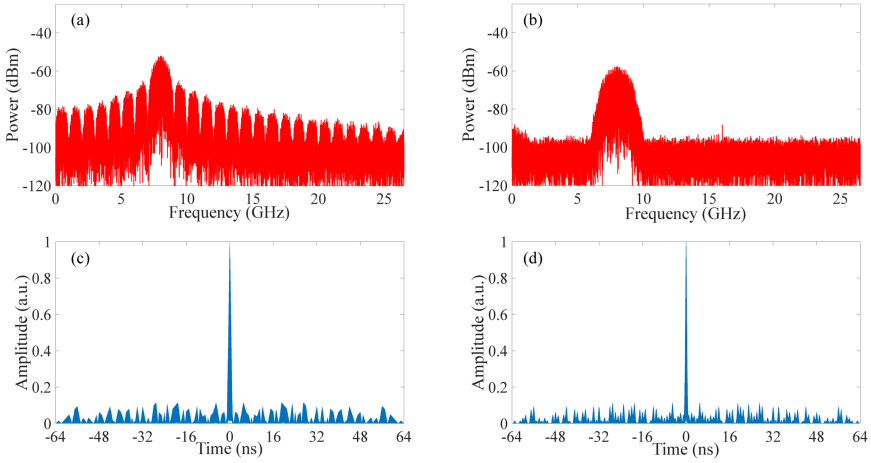

Fig. 4. Simulated electrical spectra of the frequency-doubled binary phase-coded microwave signals and the autocorrelations. (a) Spectrum when a square wave windowing function is applied. (b) Spectrum when a Gaussian windowing function is applied. (c) Autocorrelation of the generated microwave waveform when a square wave windowing function is applied. (d) Autocorrelation of the generated microwave waveform when a Gaussian windowing function is applied.

frequency-doubled phase-coded signal without and with a Gaussian windowing function. The pulse widths are 1.02 ns and 0.52 ns, with the corresponding PCRs being 63 and 123, respectively, demonstrating an increase in the PCR by almost 2 times thanks to the increase in the spectrum width when applying a Gaussian windowing function to the generated microwave waveform. The simulation results confirm the proposed structure is capable of generating a phase-coded microwave pulse signal with low spectrum sidelobes and an improved PCR at the fundamental frequency and twice the frequency of the input RF tone.

Note that the proposed microwave photonic phase-coded microwave waveform generator does not involve electronic components and optical filters. Its bandwidth is only limited by the DP-QPSK modulator bandwidth and the PM bandwidth. Both the DP-QPSK modulator and the PM are $LiNbO_3$ electro-optic modulators, which can be made to have a bandwidth of 100 GHz or greater [19]. The carrier frequency of the generated phase-coded microwave waveform can be switched between the fundamental and doubled frequency of the input RF tone by simply controlling the DP-QPSK modulator bias voltages, and the output signal can be in either CW or pulse mode.

Note that a few techniques for phase-coded microwave waveform generation have been reported [20]–[22]. The key difference and novelty of this approach are that the phase information of the generated waveform is dependent only on the polarity rather than the amplitude of the coding signal. This provides an additional degree of freedom by which the amplitude of the generated phase-coded microwave waveform can be tailored through adding a windowing function to the coding signal to effectively suppress the spectral sidelobes. In addition, the microwave waveform generators reported in [20]–[22] require the use of a coherent multi-wavelength light source and a balanced PD [20] or a 90° hybrid coupler [21], [22], which may increase the cost or limit the bandwidth of the entire waveform

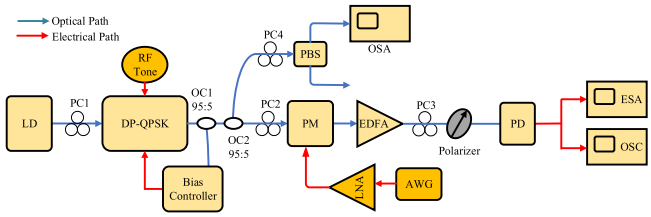

Fig. 5. Experimental setup of the phase-coded microwave waveform generator.

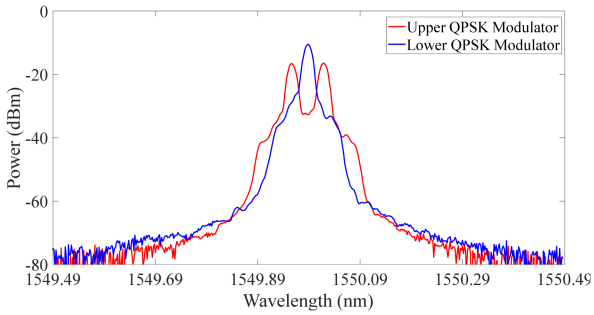

Fig. 6. Measured optical spectra at the output of the DP-QPSK modulator in two orthogonal polarization states, when the DP-QPSK modulator is biased to generate a phase-coded microwave pulse signal at the fundamental frequency of the input RF tone.

generation systems. While in the proposed approach, only a single-wavelength light source and a PD are required and no electronic components are used, which would make the system have a much wider bandwidth at a lower cost.

IV. Experimental Results

An experiment is conducted with the setup shown in Fig. 5 to evaluate the operation of the proposed phase-coded microwave waveform generator. In the experiment, the LD (IDPhotonics CoBriteDX1) is used to generate a CW optical carrier at 1550 nm with 15 dBm optical power. The DP-QPSK modulator is a commercial device with a bandwidth of 23 GHz from Fujitsu (FTM7977HQA). A polarization controller (PC1) is employed between the LD and the DP-QPSK modulator to align the polarization state of the CW light to the slow axis of the DP-QPSK modulator, to minimize the polarization-dependent loss. MZM1 in the DP-QPSK modulator is driven by a 4 GHz RF tone from an RF signal generator (Hittite HMC-T2220) and the modulation index is 0.1. A small portion of the DP-QPSK modulator output is injected into a bias controller (PlugTech MBC-DPIQ-01) via a 95:5 optical coupler (OC), to stabilize the operation of the DP-QPSK. Another small portion of the DP-QPSK modulator output is coupled out via another 95:5 OC to monitor the optical spectrum on an optical spectrum analyzer (OSA). The PM from Thorlabs (LN53S-FC) with a bandwidth of 10 GHz, which can support both TE and TM modes, is driven by a phase coding signal from an arbitrary waveform generator (AWG) (Tektronix AWG70002A). The phase coding signal is a 64-bit PRBS code followed by 22 “0” bits. The bit rate of the phase coding signal is 1 Gbit/s and its amplitude is 200 mV. Note that a second PC (PC2) is employed before the PM to

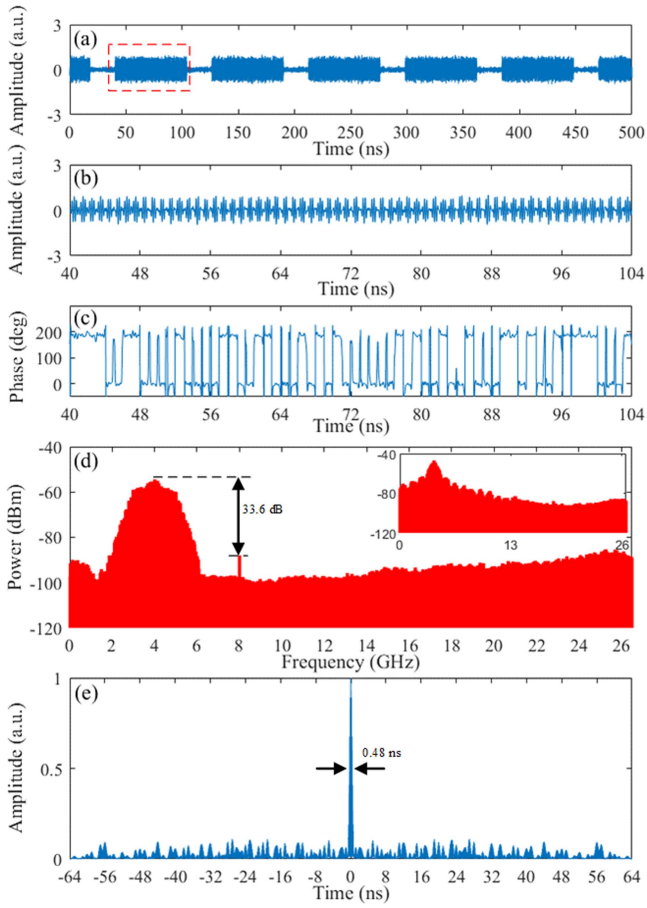

Fig. 7. Experimentally generated binary phase-coded microwave waveform and the autocorrelation. (a) The generated phase-coded microwave waveform. (b) A segment of the generated phase-coded microwave waveform from 40 to 104 ns (red dotted box in (a)). (c) Phase information extracted from the generated phase-coded microwave waveform. (d) Spectrum of the generated phase-coded microwave waveform when a Gaussian windowing function is applied. (e) Autocorrelation of the generated phase-coded microwave waveform when a Gaussian windowing function is applied. The inset of Fig. 7(d) shows the spectrum of the generated phase-coded microwave waveform when using a square wave coding signal.

align the orthogonally polarized sidebands and the carrier from the DP-QPSK modulator to the TE and TM mode, respectively. The two PCs (PC1 and PC2) are not needed if polarization maintaining components are employed. An erbium-doped fiber amplifier (EDFA) is connected to the output of the PM to compensate for the system loss. A third PC (PC 3) followed by a linear polarizer is connected at the output of the EDFA. Since the sidebands and the optical carrier are in orthogonal polarization states, PC3 is adjusted until the power of the optical carrier reduced by 3 dB from its maximum value to ensure the polarization directions of the sidebands and the optical carrier to have an angle of 45° relative to the principal axis of the polarizer. The sidebands and the optical carrier at the output of the linear polarizer, which are co-polarized, are detected at a 50-GHz PD (U2t XPDV2120R). The generated microwave waveform is monitored by an electrical spectrum analyzer (ESA) (Keysight N9020B) and an oscilloscope (OSC) (Keysight MSOV334A) via an RF splitter to simultaneously monitor the output signal in the frequency and time domains.

TABLE II
SUMMARY OF THE AUTOCORRELATION PULSE WIDTHS, PCRS, AND AUTOCORRELATION PEAK-TO-SIDELOBE RATIO (PSR) FOR THE FOUR SIMULATED PHASE-CODED MICROWAVE WAVEFORMS SHOWN IN FIGS. 3 AND 4

64-bit PRBS code	4 GHz phase-coded signal		8 GHz phase-coded signal	
	Square wave coding signal	Gaussian-windowed coding signal	Square wave coding signal	Gaussian-windowed coding signal
Pulse width	1.02 ns	0.48 ns	1.02 ns	0.52 ns
PCR	62	132	63	123
PSR	9.57 dB	9.03 dB	9.48 dB	9.17 dB

TABLE III
SUMMARY OF THE PULSE WIDTH, PCR, AND PSR FOR THE GENERATED PHASE-CODED MICROWAVE WAVEFORMS SHOWN IN FIGS. 7 AND 9

64-bit PRBS code	4 GHz phase-coded signal		8 GHz phase-coded signal	
	Square wave coding signal	Gaussian-windowed coding signal	Square wave coding signal	Gaussian-windowed coding signal
Pulse width	1 ns	0.48 ns	1.02 ns	0.49 ns
PCR	64	133	63	131
PSR	9.22 dB	9.07 dB	9.24 dB	8.91 dB

TABLE IV
SUMMARY OF THE PULSE WIDTH, PCR, AND PSR FOR THE GENERATED PHASE-CODED MICROWAVE WAVEFORMS SHOWN IN FIG. 10

13-bit Barker code	10 GHz phase-coded signal		20 GHz phase-coded signal	
	Square wave coding signal	Gaussian-windowed coding signal	Square wave coding signal	Gaussian-windowed coding signal
Pulse width	1.01 ns	0.48 ns	1.06 ns	0.5 ns
PCR	12.9	27.4	12.2	26.3
PSR	9.82 dB	9.73 dB	9.51 dB	9.14 dB

The bias voltages to the DP-QPSK modulator are adjusted via the bias controller to obtain the required bias angles given in Table I, to generate a phase-coded signal at the fundamental frequency of the input RF tone. Since the optical signals in the upper and lower paths of the DP-QPSK modulator are orthogonally polarized, the spectrums of the two orthogonally polarized optical signals can be observed separately on the OSA by adjusting PC4 in front of a PBS to pass only one of the two optical signals. Fig. 6 shows the spectrum of the first order sidebands with suppressed carrier generated by the upper QPSK modulator. The spectrum of the optical carrier at the output of the lower QPSK modulator is also shown in Fig. 6. The phase coding signal is generated by the AWG. By programing the AWG, a Gaussian window with a width factor of 2.5 is imposed to the coding signal. After adjusting the PCs before the PM and the polarizer, a phase-coded signal is generated, and it is recorded in the OSC. Fig. 7(a) shows the generated phase-coded microwave signal with a time span of 500 ns. Fig. 7(b) and (c) shows, respectively, the phase-coded signal in a 64-ns duration (from 40 to 104 ns) and its phase information recovered using Hilbert transform. As can be seen from Fig. 7(c), a binary phase shift of π is coded successfully. Fig. 7(d) shows the electrical spectrum of the generated phase-coded signal measured by the ESA. It can be seen all the sidelobes are suppressed and are below the noise floor. There is a frequency component at 8 GHz, which is the second harmonic of the RF tone generated due to the nonlinearity of the system. At the baseband, a wide spectrum is

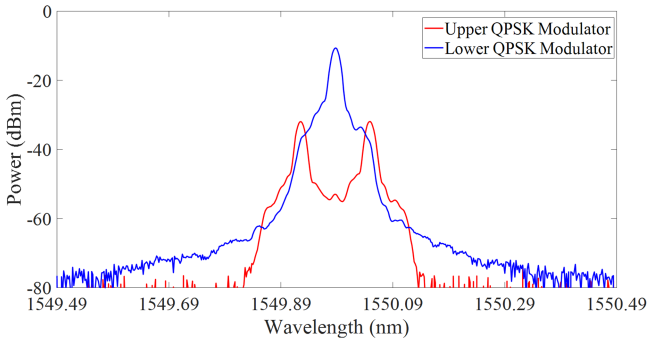

Fig. 8. Measured optical spectra at the output of the DP-QPSK modulator in two orthogonal polarization states, when the DP-QPSK modulator is biased to generate a phase-coded microwave waveform at twice the frequency of the input RF tone.

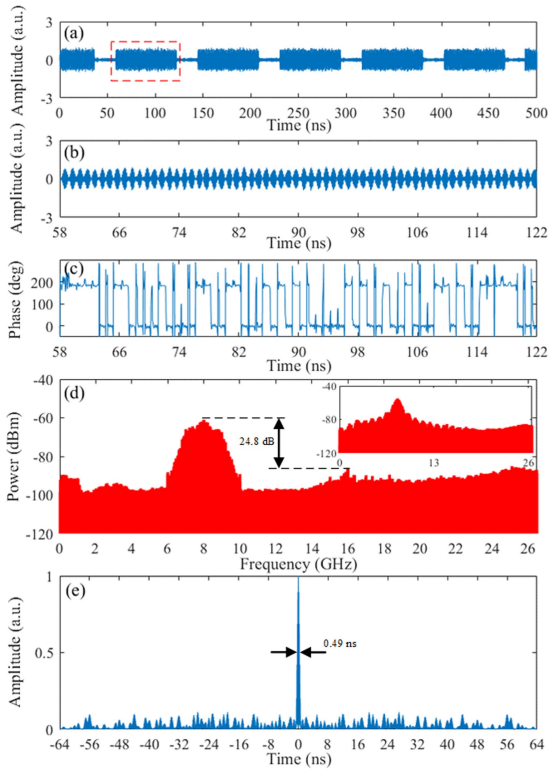

Fig. 9. Experimentally generated frequency-doubled binary phase-coded microwave waveform and the autocorrelation. (a) The generated phase-coded microwave waveform. (b) A segment of the generated phase-coded microwave waveform from 58 to 122 ns (red dotted box in (a)). (c) Phase information extracted from the generated phase-coded microwave waveform. (d) Spectrum of the generated phase-coded microwave waveform when a Gaussian windowing function is applied. (e) Autocorrelation of the generated phase-coded microwave waveform when a Gaussian windowing function is applied. The inset of Fig. 9(d) shows the spectrum of the generated frequency-doubled phase-coded microwave waveform when using a square wave coding signal.

also observed, which is resulted from the residual optical carrier that is not fully suppressed at the upper QPSK modulator output due to a limited extinction ratio of the modulator. Nevertheless, they are more than 33.6 dB below the mainlobe. Fig. 7(e) shows the autocorrelation of the phase-coded signal when using a Gaussian-windowed coding signal. The pulse width of the autocorrelation peak is 0.48 ns. This results in a PCR of 133

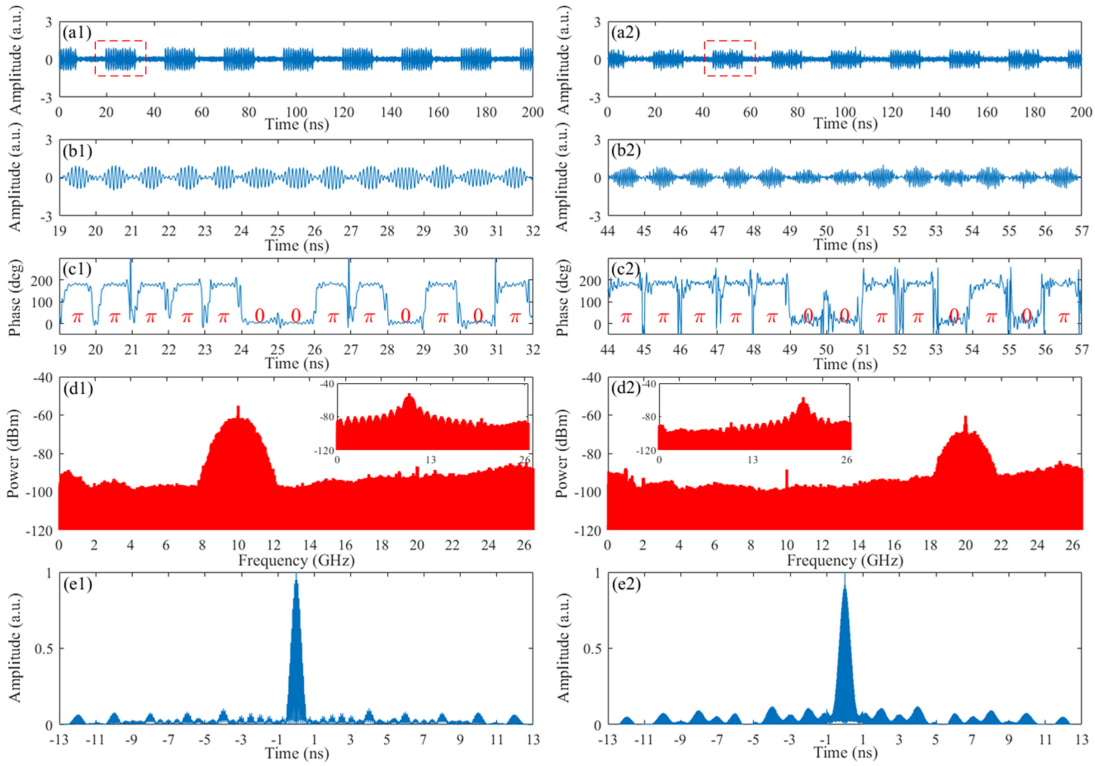

Fig. 10. Experimentally generated binary phase-coded microwave waveform and the autocorrelation at the fundamental (left) and doubled (right) input RF tone frequency. The generated phase-coded microwave waveforms at (a1) the fundamental, and (a2) the doubled frequency. A segment of the generated phase-coded microwave waveforms from (b1) 19 to 32 ns (red dotted box in a1), and (b2) 44 to 57 ns (red dotted box in a2). The recovered phase information for the phase-coded microwave waveforms at (c1) the fundamental and (c2) doubled frequency. The spectrums of the phase-coded microwave waveforms at (d1) the fundamental and (d2) doubled frequency (e) Autocorrelations of the generated phase-coded microwave waveforms at (e1) the fundamental and (e2) doubled frequency when a Gaussian windowing function is applied. The insets of Fig. 10(d1) and (d2) are obtained using a square wave coding signal.

for a 64-bit PRBS input coding signal. The peak-to-sidelobe ratio (PSR) obtained from the autocorrelation is 9.07 dB. They are in excellent agreement with the simulation results shown in Table II. For comparison, the Gaussian window is removed from the input coding signal. Therefore, the coding signal into the PM is a square-wave 64-bit PRBS code followed by 22 "0" bits. The electrical spectrum of the generated phase-coded signal is shown in the inset of Fig. 7(d). As can be seen the generated phase-coded signal has much higher sidelobes, and the mainlobe to the first sidelobe ratio is only 13.8 dB. The PCR and PSR obtained from the autocorrelation of the phase-coded signal generated by the square-wave coding signal are 64 and 9.22 dB, respectively.

The short-term and long-term stability of the system are also studied. To study the short-term stability, we allow the experimental system to operate in a lab environment for 10 minutes. No obvious changes in the generated waveform and its spectrum are observed. The long-term stability is mainly affected by the bias drift since six DC bias voltages are used to control the DP-QPSK modulator. A solution is to use two IQ modulator bias controllers [23], with each to control three bias points of the IQ modulator. Thus, long-term stable operation of the proposed waveform generator is ensured.

Then, the bias voltages to the DP-QPSK modulator are adjusted to realize frequency-doubled phase-coded microwave waveform generation. The system parameters as well as the power and frequency of the input RF tone and coding signal remain the same as for phase-coded microwave waveform generation at the fundamental frequency. The spectra of the optical signal from the upper and lower QPSK modulators are measured at the outputs of the PBS and shown in Fig. 8. As can be seen, two second order sidebands are generated by the upper QPSK modulator and an optical carrier is obtained from the lower QPSK modulator. The generated phase-coded microwave pulse signal is measured by the OSC and is shown in Fig. 9(a) and (b). Fig. 9(c) shows the phase information recovered using Hilbert transform. The electrical spectrum of the generated frequency-doubled phase-coded microwave waveform is shown in Fig. 9(d). As can be seen, the microwave carrier frequency is doubled at 8 GHz. Again, the sidelobes are largely suppressed compared with those using a square wave coding signal, as shown in the inset of Fig. 9(d). The pulse width, PCR and PSR obtained from the autocorrelation of the phase-coded signal shown in Fig. 9(e) are 0.49 ns, 131, and 8.91 dB respectively, which are similar to those of the generated phase-coded signal at the fundamental frequency and agree well with the simulation results. A comparison of the performance of the phase-coded microwave waveform generator when using a square wave coding signal and a Gaussian-windowed coding signal is shown in Table III, confirming the improvement in both

sidelobe suppression and PCR when using a windowed phase coding signal. It should be noted that the phase-coded microwave waveform at twice the input RF tone frequency is generated by only adjusting the bias voltages of the DP-QPSK modulator. Therefore, a fundamental-frequency and doubled-frequency phase-coded signal can be switched without any physical change in the system.

Finally, to verify that the system can be used for different types of coding signals and has a wide frequency tunability, the input coding signal is changed to a Gaussian-windowed 1 Gbit/s 13-bit Barker code followed by 22 "0" bits and the frequency of the input RF tone is tuned to 10 GHz. Phase-coded microwave waveforms with low spectrum sidelobes at the fundamental frequency and the doubled frequency are obtained, as shown in Fig. 10(a1) and (a2). A segment of the generated phase-coded microwave waveforms from 19 to 32 ns, and 44 to 57 ns, are shown in Fig. 10(b1) and (b2), respectively. The recovered phase information for the phase-coded microwave waveforms at the fundamental and doubled frequencies are shown in Fig. 10(c1) and (c2). The spectrums of the phase-coded microwave waveforms at the fundamental and doubled frequencies are shown in Fig. 10(d1) and (d2). As can be seen, the sidelobes of the spectrums are highly suppressed. As comparison, the spectrums of the generated phase-coded microwave waveforms when using a square wave coding signal are shown in the inset of Fig. 10(d1) and (d2). The pulse compression capability of the system when using a square wave coding signal and a Gaussian-windowed coding signal is evaluated, as shown in Fig. 10(e1) and (e2), and is summarized in Table IV.

Based on the experimental results, we conclude that when using a Gaussian-windowed coding signal, the generated phase-coded microwave waveform has low spectrum sidelobes with improved PCR. The system can be configured to generate phase-coded microwave waveforms at the fundamental and doubled frequencies. Since no optical filters are employed in the system, the carrier frequency of the generated phase-coded microwave waveforms can be tuned by simply tuning the frequency of the input RF tone.

V. Conclusion

A new technique to generate binary phase-coded microwave waveforms with highly suppressed spectrum sidelobes has been theoretically analyzed and experimentally demonstrated. The unique feature of the technique is that the phase shift is not dependent on the amplitude of the phase coding signal, thus providing an additional degree of freedom, which was employed to apply a windowing function to the generated phase-coded microwave waveform through a windowed phase coding signal, to reduce the sidelobes in the spectrum of the generated phase-coded signal. Since no electronic components and optical filters were employed in the system, the system can operate with a wide frequency tunable range. In addition, the frequency of the generated microwave waveform can be switched between the fundamental and the 2nd harmonic carrier frequency by simply adjusting the modulator bias voltages. To the best of our knowledge, this is the first phase-coded microwave waveform generator that provides all the above features. The operation of the system was evaluated by experiments. Experimental results showed that, using a windowed 64-bit Gaussian pseudo-random binary sequence coding signal, a phase-coded microwave waveform was generated with the sidelobes of the spectrum largely suppressed by 20 dB and a pulse compression ratio as large as 133. Generation of binary phase-coded microwave waveforms at doubled carrier frequencies was demonstrated experimentally. The frequency tunability was also demonstrated.

References

[1] M. Skolnik, "Role of radar in microwaves," *IEEE Trans. Microw. Theory Techn.*, vol. 50, no. 3, pp. 625–632, Mar. 2002.

[2] EOSpace Ultra-wideband modulator, 2022, [Online]. Available: https://www.eospace.com/ultrawideband-modulator

[3] J. P. Yao, "Microwave photonics," *J. Lightw. Technol.*, vol. 27, no. 3, pp. 314–335, Feb. 2009.

[4] R. A. Minasian, E. H. W. Chan, and X. Yi, "Microwave photonic signal processing," *Opt. Exp.*, vol. 21, no. 19, pp. 22918–22936, 2013.

[5] J. D. McKinney, D. E. Leaird, and A. M. Weiner, "Millimeter-wave arbitrary waveform generation with a direct space-to-time pulse shaper," *Opt. Lett.*, vol. 27, no. 5, pp. 1345–1347, Aug. 2002.

[6] Y. Dai and J. P. Yao, "Microwave pulse phase encoding using a photonic microwave delay-line filter," *Opt. Lett.*, vol. 32, no. 24, pp. 3486–3488, Dec. 2007.

[7] C. Wang and J. P. Yao, "Phase-coded millimeter-wave waveform generation using a spatially discrete chirped fiber Bragg grating," *IEEE Photon. Technol. Lett.*, vol. 24, no. 17, pp. 1493–1495, Sep. 2012.

[8] Z. Li, W. Li, H. Chi, X. Zhang, and J. Yao, "Photonic generation of phase-coded microwave signal with large frequency tunability," *IEEE Photon. Technol. Lett.*, vol. 23, no. 11, pp. 712–714, Jun. 2011.

[9] Z. Li, M. Li, H. Chi, X. Zhang, and J. Yao, "Photonic generation of phase-coded millimeter-wave signal with large frequency tunability using a polarization-maintaining fiber Bragg grating," *IEEE Microw. Wireless Compon. Lett.*, vol. 21, no. 12, pp. 694–696, Dec. 2011.

[10] S. Zhu, M. Li, X. Wang, N. H. Zhu, Z. Z. Cao, and W. Li, "Photonic generation of background-free binary phase-coded microwave pulses," *Opt. Lett.*, vol. 44, no. 1, pp. 94–97, Jan. 2019.

[11] W. Li, L. X. Wang, M. Ling, and N. H. Zhu, "Photonic generation of widely tunable and background-free binary phase-coded radio-frequency pulses," *Opt. Lett.*, vol. 38, no. 17, pp. 3441–3444, 2013.

[12] W. Li, L. X. Wang, M. Li, and N. H. Zhu, "Single phase modulator for binary phase-coded microwave signals generation," *IEEE Photon. Technol. Lett.*, vol. 25, no. 19, pp. 1867–1870, Oct. 2013.

[13] R. Chen and B. Cantrell, "Highly bandlimited radar signals," in *Proc. IEEE Radar Conf.*, Apr. 2002, pp. 220–226.

[14] Y. Hu, E. H. W. Chan, X. Wang, X. Feng, B. Guan, and J. Yao, "All-optical windowed binary phase-coded microwave waveform generation," in *Proc. IEEE Int. Topical Meeting Microw. Photon.*, 2021, pp. 1–4.

[15] T. Li, E. H. W. Chan, X. Wang, X. Feng, and B. Guan, "All-optical photonic microwave phase shifter requiring only a single DC voltage control," *IEEE Photon. J.*, vol. 8, no. 4, Aug. 2016, Art. no. 5501008.

[16] Y. P. Bai *et al.*, "High power efficiency and dynamic range analog photonic link with suppressed dispersion-induced power fading," *J. Lightw. Technol.*, vol. 38, no. 21, pp. 5973–5980, Nov. 2020.

[17] B. M. Haas and T. E. Murphy, "A simple, linearized, phase-modulated analog optical transmission system," *IEEE Photon. Technol. Lett.*, vol. 19, no. 10, pp. 729–731, May 2007.

[18] S. Pan and Y. Zhang, "Tunable and wideband microwave photonic phase shifter based on a single-sideband polarization modulator and a polarizer," *Opt. Lett.*, vol. 37, no. 21, pp. 4483–4485, Nov. 2012.

[19] C. Wang *et al.*, "100-GHz low voltage integrated lithium niobate modulators," in *Proc. Conf. Lasers Electro-Opt., OSA Tech. Dig.*, 2018, Paper SM3B.4.

[20] D. Wu *et al.*, "Photonic generation of multi-frequency phase-coded microwave signal based on a dual-output Mach-Zehnder modulator and balanced detection," *Opt. Exp.*, vol. 25, no. 13, pp. 14516–14523, Jun. 2017.

[21] P. Li *et al.*, "Photonic generation of binary and quaternary phase-coded microwave signals by utilizing a dual-polarization dual-parallel Mach-Zehnder modulator," *Opt. Exp.*, vol. 26, no. 21, pp. 28013–28021, Oct. 2018.

[22] W. Zhang, Q. Tan, X. Li, and D. Wang, "Photonic generation of background-free frequency-doubled phase-coded microwave pulses with immunity to periodic power fading," *Opt. Lett.*, vol. 45, no. 6, pp. 1407–1410, Mar. 2020.
[23] X. Li *et al.*, "Arbitrary bias point control technique for optical IQ modulator based on dither-correlation detection," *J. Lightw. Technol.*, vol. 36, no. 18, pp. 3824–3836, Sep. 2018.

Yang Hu received the B.E. degree in measurement and control technology and instruments from Nanchang Hangkong University, Nanchang, China, in 2019. He is currently working toward the master's degree in optical engineering with the Institute of Photonics Technology, Jinan University, Guangzhou, China. His research focuses on microwave photonic signal processing.

Erwin H. W. Chan (Senior Member, IEEE) received the B.Sc., B.Eng., (Hons.) and Ph.D. degrees from The University of Sydney, Sydney, NSW, Australia, in 1998, 2000, and 2005, respectively. He is currently an Associate Professor with the College of Engineering, IT and Environment, Charles Darwin University, Darwin, NT, Australia. From 2005 to 2014, he was a Senior Research Fellow and an External Lecturer with The University of Sydney. He has authored or coauthored more than 150 papers in international refereed journals and conferences, and has carried out consulting work with industry. His research interests include microwave photonics, optical telecommunications, optical signal processing, and photonic and microwave technology. Dr. Chan has been a member of the technical program committee of the Conference on Laser and Electro-optics. He was the recipient of The University of Sydney Early Career Development Award and Australian Postdoctoral Fellowship awarded by the Australian Research Council.

Xudong Wang received the B.E. degree in electrical engineering from the Dalian University of Technology, Dalian, China, in 2007, the M.E. and Ph.D. degrees from The University of Sydney, Sydney, NSW, Australia, in 2008 and 2014, respectively. He is currently an Associate Professor with the Institute of Photonics Technology, Jinan University, Guangzhou, China. His research focuses on microwave photonic signal processing.

Xinhuan Feng received the B.Sc., M.Sc., and Ph.D. degrees in optics from Nankai University, Tianjin, China, in 1995, 1998, and 2005, respectively. From 2005 to 2008, she was a Postdoctoral Fellow with Photonics Research Centre, The Hong Kong Polytechnic University. Since March 2009, she has been with the Institute of Photonics Technology, Jinan University, Guangzhou, China. Her research interests include various fiber active and passive devices and their applications, and microwave photonic signal processing.

Bai-Ou Guan (Fellow, Optica) received the B.Sc. degree in applied physics from Sichuan University, Chengdu, China, in 1994, and the M.Sc. and Ph.D. degrees in optics from Nankai University, Tianjin, China, in 1997 and 2000, respectively. From 2000 to 2005, he was with the Department of Electrical Engineering, The Hong Kong Polytechnic University, Hong Kong, first as a Research Associate, then as a Postdoctoral Research Fellow. From 2005 to 2009, he was with the School of Physics and Optoelectronic Engineering, Dalian University of Technology, Dalian, China, as a Full Professor. In 2009, he joined Jinan University, Guangzhou, China, where he founded the Institute of Photonics Technology. He has authored and coauthored more than 230 technical papers in peer-reviewed international journals and presented more than 30 invited talks at major international conferences. His research interests include fiber optic devices and technologies, optical fiber sensors, biomedical photonic sensing and imaging, and microwave photonics. He was the recipient of a Distinguished Young Scientist Grant from the Natural Science Foundation of China in 2012. He is a Fellow of Optica, and was the General Chair/Co-Chair, Technical Program Committee or Subcommittee Chair/Co-Chair of more than 10 international conferences.

Jianping Yao (Fellow, IEEE, Fellow, Optica) received the Ph.D. degree in electrical engineering from the Université de Toulon et du Var, Toulon, France, in December 1997. He is currently a Distinguished University Professor and the University Research Chair in microwave photonics with the School of Electrical Engineering and Computer Science (EECS), University of Ottawa, Ottawa, ON, Canada. From 1998 to 2001, he was an Assistant Professor with the School of Electrical and Electronic Engineering, Nanyang Technological University, Singapore. In December 2001, he joined the School of Electrical Engineering and Computer Science, University of Ottawa, as an Assistant Professor, where he was promoted to an Associate Professor in May 2003, and a Full Professor in May 2006. In 2007, he was appointed as the University Research Chair with Microwave Photonics. From July 2007 to June 2010 and July 2013 to June 2016, he was the Director of the Ottawa-Carleton Institute for Electrical and Computer Engineering. He has authored or coauthored more than 660 research papers, including more than 380 papers in peer-reviewed journals, and more than 280 papers in conference proceedings. Prof. Yao was the Editor-in-Chief of the IEEE PHOTONICS TECHNOLOGY LETTERS 2017–2021, a Topical Editor of *Optics Letters* 2015–2017, an Associate Editor for the *Science Bulletin* 2016–2018, a Steering Committee Member of the IEEE JOURNAL OF LIGHTWAVE TECHNOLOGY 2016–2021, and has been an Advisory Editorial Board member of *Optics Communications* since 2014. In 2013, he was a Guest Editor of a Focus Issue on Microwave Photonics in *Optics Express*, a Lead-Editor of a Feature Issue on Microwave Photonics in *Photonics Research* in 2014, and a Guest Editor of a special issue on Microwave Photonics in IEEE/OSA JOURNAL OF LIGHTWAVE TECHNOLOGY in 018. Prof. Yao was the Technical Committee Chair of IEEE MTT-S Microwave Photonics 2016–2021 and an elected member of the Board of Governors of the IEEE Photonics Society 2019–2021. Prof. Yao was a member of the European Research Council Consolidator Grant Panel in 2016, 2018, and 2020, the Qualitative Evaluation Panel in 2017, and a panelist of the National Science Foundation Career Awards Panel in 2016. Prof. Yao was the Chair of numerous international conferences, symposia, and workshops, including the Vice Technical Program Committee (TPC) Chair of the 2007 IEEE Topical Meeting on Microwave Photonics, TPC Co-Chair of the 2009 and 2010 Asia-Pacific Microwave Photonics Conference, TPC Chair of the high-speed and broadband wireless technologies subcommittee of the IEEE Radio Wireless Symposium 2009–2012, TPC Chair of the microwave photonics subcommittee of the IEEE Photonics Society Annual Meeting 2009, TPC Chair of the 2010 IEEE Topical Meeting on Microwave Photonics, General Co-Chair of the 2011 IEEE Topical Meeting on Microwave Photonics, TPC Co-Chair of the 2014 IEEE Topical Meetings on Microwave Photonics, General Co-Chair of the 2015 and 2017 IEEE Topical Meeting on Microwave Photonics, and General Chair of the 2019 IEEE Topical Meeting on Microwave Photonics. He was also a committee member for a number of international conferences, such as IPC, OFC, CLEO, BGPP, and MWP. Prof. Yao was the recipient of the 2005 International Creative Research Award of the University of Ottawa, and 2007 George S. Glinski Award for Excellence in Research. In 2008, he was awarded a Natural Sciences and Engineering Research Council of Canada Discovery Accelerator Supplements Award. Prof. Yao was selected to receive an inaugural OSA Outstanding Reviewer Award in 2012 and was one of the top ten reviewers of IEEE/OSA JOURNAL OF LIGHTWAVE TECHNOLOGY 2015–2016. Prof. Yao was an IEEE MTT-S Distinguished Microwave Lecturer for 2013–2015. He was the recipient of the 2017–2018 Award for Excellence in Research of the University of Ottawa, and was the recipient of the 2018 R.A. Fessenden Silver Medal from IEEE Canada. Prof. Yao is a registered Professional Engineer of Ontario. He was elected as a Fellow of the Optica (formerly Optical Society of America) in 2010, Canadian Academy of Engineering in 2012, and Royal Society of Canada in 2018. In June 2016, Prof. Yao was conferred the title of Distinguished University Professor of the University of Ottawa.